Pergamon

www.neuroscience-ibro.com

PII: S0306-4522(01)00506-1

Neuroscience Vol. 110, No. 3, pp. 459–473, 2002

0306-4522/02 $22.00+0.00

ELECTROPHYSIOLOGICAL AND MORPHOLOGICAL PROPERTIES OF CELL TYPES IN THE CHICK NEOSTRIATUM CAUDOLATERALE

S. KRÖNER,[a]* K. GOTTMANN,[b] H. HATT[b] and O. GÜNTÜRKÜN[a]

[a]AE Biopsychologie, Fakultät für Psychologie, Ruhr-Universität Bochum, 44780 Bochum, Germany

[b]Lehrstuhl für Zellphysiologie, Fakultät für Biologie, Ruhr-Universität Bochum, 44780 Bochum, Germany

Abstract—The neostriatum caudolaterale, in the chick also referred to as dorsocaudal neostriatal complex, is a polymodal associative area in the forebrain of birds that is involved in sensorimotor integration and memory processes. We have used whole-cell patch-clamp recordings in chick brain slices to characterize the principal cell types of the neostriatum caudolaterale. Electrophysiological properties distinguished four classes of neurons. The morphological characteristics of these classes were examined by intracellular injection of Lucifer Yellow. Type I neurons characteristically fired a brief burst of action potentials. Morphologically, type I neurons had large somata and thick dendrites with many spines. Type II neurons were characterized by a repetitive firing pattern with conspicuous frequency adaptation. Type II neurons also had large somata and thick dendrites with many spines. There was no clear morphological distinction between type I and type II neurons. Type III neurons showed high-frequency firing with little accommodation and a prominent time-dependent inward rectification. They had thin, sparsely spiny dendrites and extensive local axonal arborizations. Electrophysiological and morphological properties indicated them as being interneurons. Type IV neurons had a longer action potential duration, a larger input resistance, and a longer membrane time constant than the other classes. Type IV neurons had small somata and short dendrites with few spines. The long axon collaterals of neurons in all spiny cell classes (types I, II, IV) followed similar patterns, suggesting that neurons from all these types can contribute to the projections of the neostriatum caudolaterale to sensory, limbic and motor areas.

The electrophysiological and anatomical characterization of the major classes of neurons in the caudal forebrain of the chick provides a framework for the investigation of sensorimotor integration and learning at the cellular level in birds.

Key words: forebrain, whole-cell recordings, immunocytochemistry, sensorimotor integration.

The neostriatum caudolaterale (NCL), in the chick also referred to as dorsocaudal neostriatal complex (Metzger et al., 1998), is a multimodal association area in the forebrain of birds (Leutgeb et al., 1996; Metzger et al., 1998; Kröner and Güntürkün, 1999). In the chick it has mainly been studied as part of a network responsible for early learning, specifically imprinting (Bock et al., 1997; Metzger et al., 1998; Bock and Braun, 1999a,b), whereas in the pigeon most work has focused on tasks which in mammals invoke 'frontal' executive functions, e.g. working memory (Mogensen and Divac, 1982, 1993; Gagliardo et al., 1996, 1997; Güntürkün, 1997; Kalt et al., 1999), reversal learning (Hartmann and Güntürkün, 1998; Diekamp et al., 2000), response inhibition (Güntürkün, 1997; Aldavert-Vera et al., 1999), and spatial orientation (Gagliardo and Divac, 1993). Anatomically, the NCL seems to be particularly well suited for the association between external stimuli and the animal's behavior, as it integrates information from all modalities and exerts influence over motor and limbic structures (Metzger et al., 1998, in chicks; Leutgeb et al., 1996; Kröner and Güntürkün, 1999, in pigeons). In the chick, the NCL has therefore been postulated to be a polymodal associative part of the 'imprinting pathway', in which the various sensory and emotional components of natural imprinting objects are integrated during both the learning process and memory recall (Braun et al., 1999).

With regard to short-term memory and executive functions recent electrophysiological studies have begun to unravel the cellular mechanisms that underlie these functions of the NCL. Single-unit recordings in awake pigeons performing a delayed Go/No-Go task have demonstrated the involvement of NCL neurons in response inhibition and working memory (Kalt et al., 1999). The maintenance of information 'on-line' during short intervals is an essential component of working memory. In standard delayed response tasks domestic chickens show a similar performance as pigeons when short delays (1.5 s) are used (Foster et al., 1995). However, this interval can be drastically extended when social stimuli instead of food reinforcement are used. Five-day-old chicks accustomed to follow an imprinted object can

*Correspondence to: S. Kröner, Department of Neuroscience, University of Pittsburgh, 446 Crawford Hall, Pittsburgh, PA 15260, USA. Tel.: +1-412-624-4567; fax: +1-412-624-9198.

E-mail address: svk4@pitt.edu (S. Kröner).

Abbreviations: AHP, afterhyperpolarization; ANOVA, analysis of variance; EGTA, ethylene glycol-bis(2-aminoethyl-ether)-*N*,*N*,*N*′,*N*′-tetraacetic acid; HEPES, *N*-(2-hydroxyethyl)piperazine-*N*′-(2-ethanesulfonic acid); LY, Lucifer Yellow; NCL, neostriatum caudolaterale; Nd, neostriatum dorsale; PBS, phosphate-buffered saline; RMP, resting membrane potential.

remember it's location over delay periods of up to 180 s (Vallortigara et al., 1998).

Similar to the modules of mammalian cortex (Douglas and Martin, 1992), the avian forebrain might be constructed from a relatively small number of canonical circuits, that are repeated in large quantities to achieve parallel computing power. Thus, to further extend our understanding of the functions of the NCL on a cellular level, it is important to characterize its intrinsic neuronal organization and the cell types that might be involved in the processing of different aspects of information. In this report, we have used *in vitro* whole-cell patch-clamp recording in combination with intracellular staining to characterize the principal cell types in the chick NCL electrophysiologically and morphologically.

EXPERIMENTAL PROCEDURES

Preparation of slices and electrophysiological recording

Fertilized eggs were obtained from a commercial supplier (Sörries Trockels, Möhnesee, Germany) and chicks (*Gallus gallus*) were hatched and kept in small groups on a 12:12 h dark/light cycle. All efforts were made to minimize both the suffering and number of animals used. Treatment of the animals conformed to German guidelines and was approved by a review committee of the State of North Rhine-Westphalia, Germany (Az 23.8720–27.7). A total of 43 chicks (7–11 days post-hatch, mean 9.1 days) were decapitated and the brains were transferred to iced extracellular solution. Coronal slices (350 μm) of the caudal telencephalon were cut on a vibratome. Slices were incubated in extracellular solution consisting of (in mM): 119 NaCl, 2.5 KCl, 1 NaH_2PO_4, 26.2 $NaHCO_3$, 10 D-glucose, 3.5 $CaCl_2$, and 1.3 $MgCl_2$, saturated with 95% O_2/5% CO_2, pH 7.3. Slices were allowed to recover for at least 1 h, before being transferred to the recording chamber. Recordings were made at room temperature (22–24°C) in a submerged slice chamber perfused with extracellular solution.

Whole-cell patch-clamp recordings were obtained in the caudolateral subventricular region of the forebrain (cf. Fig. 1), using the blind-patch technique. In current-clamp experiments recording electrodes (4–7 MΩ resistance) were filled with an intracellular solution consisting of (in mM): 135 K-gluconate, 20 KCl, 2 $MgCl_2$, 10 HEPES, 0.1 EGTA, 4 Na_2-ATP, and 0.5 Na_2-GTP, and adjusted to pH 7.3 with KOH. In some recordings 3 mg/ml of the dipotassium salt Lucifer Yellow (LY; Sigma, Deisenhofen, Germany) was added to the intracellular solution and neurons were filled by diffusion during 30–90 min of recording. Recordings were made using a HEKA (Lambrecht, Pfalz, Germany) EPC-7 patch-clamp amplifier, filtered at 3 kHz, and sampled at 20 kHz. The voltage drop across the pipette (which was usually about 8–10 mV) could not be bridge-balanced. Sampling was done with a Digidata 1200 interface using pClamp 6.0 software (Axon Instruments, Foster City, CA, USA), and data were stored on computer for off-line analysis with the CLAMPFIT module of pClamp. Input resistance was determined from the voltage deflection induced by a hyperpolarizing current pulse in the linear range of the current–voltage relation. Membrane time constants were calculated by fitting a single exponential function to the voltage response to injections of hyperpolarizing currents in the linear range of the voltage response. The percentage sag that occurred in some neurons in response to hyperpolarizing and depolarizing current pulses was calculated as $100\times(V_{max}-V_{end})/V_{max}$, where V_{max} was the peak voltage deflection and V_{end} the voltage at the end of the current pulse. Resting membrane potentials (RMPs) were assessed in current-clamp mode 3–5 min after establishing the whole-cell configuration. Spike duration was measured at the half-maximal amplitude from threshold, and the amplitude and time-to-peak value for the afterhyperpolarization (AHP) which followed the action potential were measured from the equipotential point on the repolarizing phase.

Histological procedures

Following recording, slices were fixed in 4% paraformaldehyde and 0.2% glutaraldehyde in 0.12 M phosphate buffer (4°C, pH 7.4) for about 15 h. They were then transferred to a solution of 30% sucrose in phosphate buffer containing 0.9% NaCl (phosphate-buffered saline (PBS); pH 7.4) and 0.01% NaN_3 as a preservative. Slices were resectioned at 70 μm on a freezing microtome and collected in PBS. For immunohistochemistry of LY, endogenous peroxidases were blocked by preincubating slices in 0.5% H_2O_2. Slices were washed in PBS and floating sections were incubated overnight at 4°C in biotinylated anti-LY from rabbit (Molecular Probes, Leiden, The Netherlands; 1:200 working dilution) in PBS containing 0.3% Triton X-100 (Sigma). After washing, slices were incubated for 2 h in the avidin–biotin complex (Vector Laboratories, Burlingame, CA, USA; 1:100 in PBS with 0.3% Triton X-100). Washes in PBS were followed by additional washes in 0.12 M acetate buffer (pH 6). Staining was achieved by the 3,3′-diaminobenzidine technique with heavy-metal amplification by adding $H_8N_2NiO_8S_2$ (2.5 g/100 ml), NH_4Cl and $CoCl_2$ (both 40 mg/100 ml). After 20 min of preincubation the reaction was catalyzed using 0.3% H_2O_2. Rinsing the tissue in acetate buffer and PBS stopped the reaction. Slices were then mounted, dehydrated and coverslipped.

Quantitative measures of cell morphology were made using a Leica DMR (Leica, Wetzlar, Germany) and the analySIS software package (Soft-Imaging Software, Münster, Germany). These analyses were limited to those cells in which the majority of the dendritic arbor was preserved after resectioning. Dendritic length was measured at ×25 or ×50 magnification and spines were counted at ×125 magnification. Measurements for the area covered by a neuron's dendrites and the dendritic field diameter were obtained by aligning images of all sections and subsequently 'connecting' the tips of the dendrites. This proved valid, especially as most neurons – with the exception of few type IV neurons – had symmetrical dendritic fields. For some cells camera lucida reconstructions were drawn using a Leitz BioMed with a drawing tube at ×12.5 or ×50 magnification.

Data analysis. Data are presented as means ± S.E.M. Statistical analyses were done using the SPSS 8.0 software package. The differences among cell classes for the various parameters were compared by analysis of variance (ANOVA) and the statistical significance of the differences ($P<0.05$) was examined with a Scheffe test for multiple comparisons.

RESULTS

Stable whole-cell recordings were obtained from 136 cells in the NCL. Neurons were selected only if they exhibited a RMP more negative than −55 mV and an overshooting action potential. Neurons were classified into four distinct types according to qualitative differences in their intrinsic firing properties and in the voltage responses to hyperpolarizing current pulses. For 70 of the neurons thus characterized basic morphological features were analyzed after filling with LY. The two main cell types (types I and II) could not be distinguished with regard to their morphological characteristics. The distribution of cell types did not vary throughout the NCL (Fig. 1).

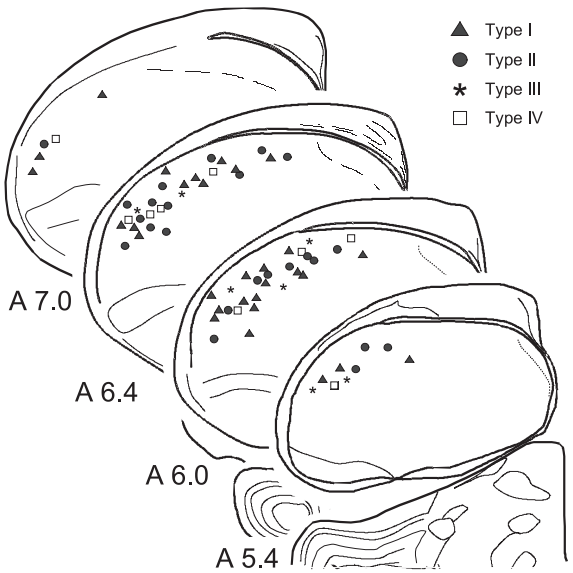

Fig. 1. Distribution of 70 neurons in the chick NCL that were characterized both electrophysiologically and morphologically. Cells were classified according to their electrophysiological properties.

Type I neurons

Type I cells displayed a characteristic firing pattern that consisted of a single action potential or a brief burst of spikes. Type I cells represented 56 of the 136 cells characterized (41%).

Firing properties. Type I cells were marked with their tendency to fire a single action potential or two to eight clustered spikes at high frequency at the onset of depolarizing pulses (Fig. 2A). After the end of these 'bursts', type I neurons typically did not fire further action potentials during prolonged (1.1 s) depolarization. The number of action potentials in a burst and the instantaneous spike frequency varied with regard to the current amplitude injected (Fig. 2A, C). However, in the course of other experiments spontaneous occurring all-or-none bursts were found both in type I and type II neurons (see below) when fast GABAergic inhibition was abolished in the slice by adding picrotoxin (100 µM) to the extracellular solution (data not shown). In these spontaneous bursts usually four to six spikes rode on a depolarizing envelope that was followed by an AHP of long duration (tens to hundreds of ms).

In type I cells the threshold for firing an action potential occurred at relatively high depolarized potentials, especially in relation to their negative RMP (Table 1). Type I cells varied with respect to their behavior in the subthreshold voltage range: in response to subthreshold depolarizing current pulses the majority of type I cells (38 of 56) showed prominent low-threshold potentials that were not seen in the remaining neurons (cf. Fig. 2A1, A2). Furthermore, most of the cells that showed these transient 'hump'-like depolarizing responses also displayed a complex pattern of afterpotentials that followed the first spikes. These consisted of an initial, fast AHP that was followed by an intercalated depolarizing afterpotential and a late medium-duration AHP (see Fig. 2A1). The remaining type I cells showed only a monophasic AHP (cf. Fig. 2A2).

Membrane rectification. Type I cells had low apparent input resistances and intermediate membrane time constants (Table 1). In response to hyperpolarizing current pulses that drove the membrane potential more negative than about −80 mV, all type I neurons showed a pronounced fast-activated inward rectification resulting in an upward bend in the current–voltage relation (Fig. 2D). Most type I cells also showed membrane outward rectification at the end of the current pulse, resulting in a downward bend in the *I–V* plot at depolarized potentials (Fig. 2A).

Morphology. Of the 56 physiologically characterized type I cells 30 were successfully recovered and morphologically reconstructed. Single or burst firing neurons had large round or fusiform somata (diameter 15–22 µm; Table 2) and multipolar arranged dendrites. Dendrites were usually long (dendritic field diameters 230–328 µm; Table 2) and displayed medium to high spine densities (Figs. 2B, 7A, B and 8). The axon branched near the soma and gave rise to thin collaterals that ramified in a loose local plexus (Figs. 2B, 7A and 8). In addition to these recurrent collaterals which displayed numerous varicose-like swellings, often two to five longer collaterals were observed that projected outside the NCL (cf. Fig. 2B, insert). These axonal arborizations showed less varicosities and followed one of three general directions: In most cases one to three collaterals moved ventrally within the plane of the slice to terminate within the underlying archistriatum. Other collaterals traveled through the NCL either dorsomedially, towards the auditory subunit of the NCL, the neostriatum dorsale (Nd), and possibly other sensory forebrain areas, or ventromedially, in the direction of the basal ganglia (cf. Metzger et al., 1998; Kröner and Güntürkün, 1999). Ventromedially directed arborizations, however, could be followed only over relatively short distances before they left the sagittal plane of the slice.

Type II neurons

Type II cells were characterized by their repetitive firing pattern. They represented 49 of the 136 neurons studied (36%).

Firing properties. Most characteristics of the first action potential were similar to those found in type I neurons (Table 1). In contrast to type I neurons, however, type II neurons had a significantly xmore depolarized RMP. More importantly, relatively small somatically injected depolarizing current pulses readily elicited tonic firing in type II cells. Two typical examples of type II cells are shown in Fig. 3A. Current pulses that depolarized type II cells just above threshold usually evoked a single action potential that often had long latencies. With larger depolarizing currents a pattern of

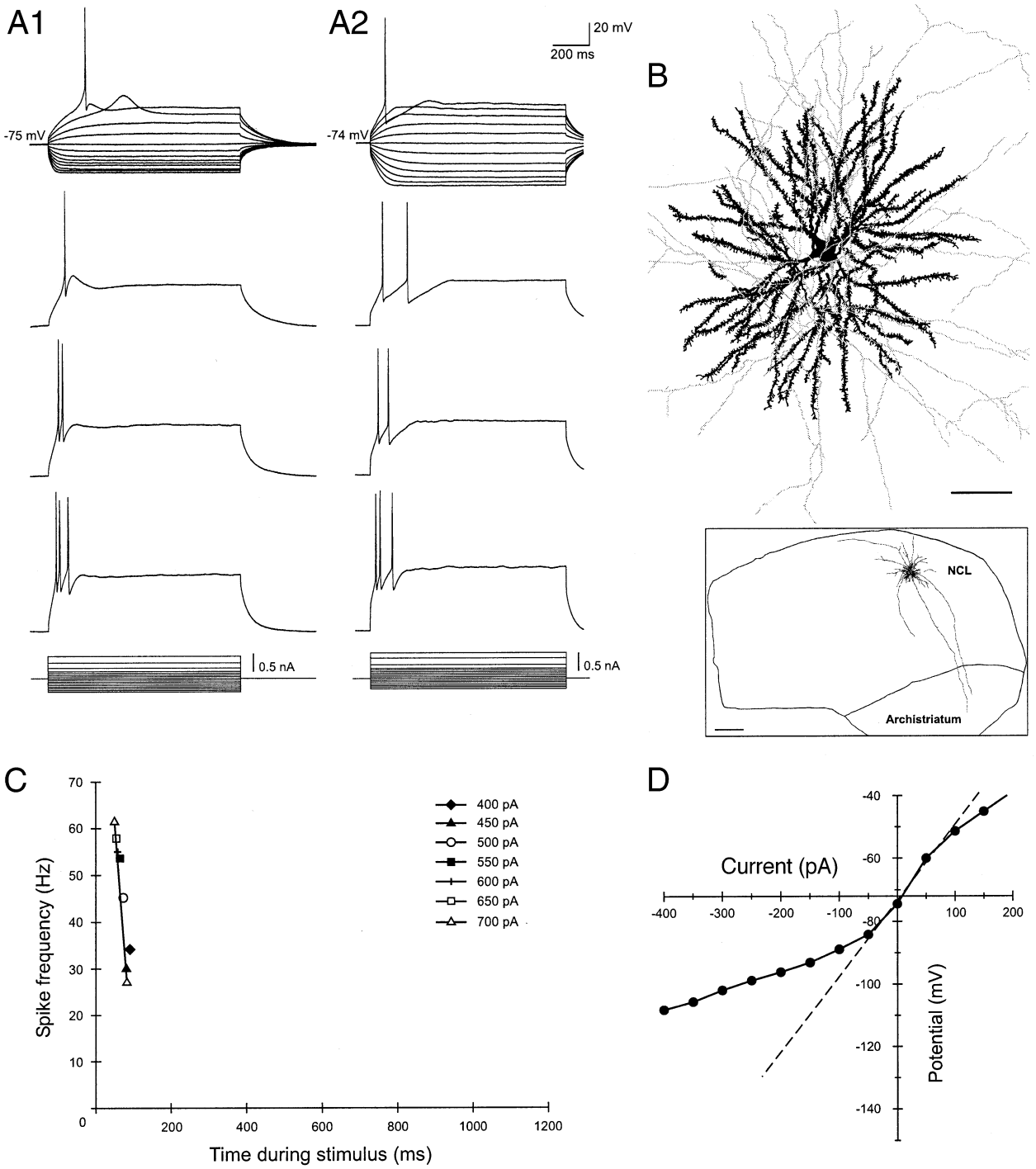

Fig. 2. Intrinsic firing properties and membrane rectification of type I neurons. (A) Examples of voltage responses to hyperpolarizing and depolarizing current pulses (−400–700 pA in A1 and −300–800 pA in A2) in two neurons that showed rapid adaptation of action potential firing. Type I cells typically responded with 'bursts' of action potentials to current pulses of increasing intensity. Both cells show membrane inward rectification to relatively large hyperpolarizing currents and outward rectification to depolarizing currents in the spike threshold range. The cell in A1 displays a prominent subthreshold 'hump'-like potential and a depolarizing afterpotential following single spikes. The cell in A2 shows only monophasic AHPs of comparatively long duration. Note that there is also apparently less membrane rectification in this cell than in the cell shown in A1. (B) Camera lucida reconstruction of a type I neuron. The soma and dendrites are drawn in black; the axon collaterals are shown in gray. Scale bar = 50 μm. Insert: location of the same cell in the caudal neostriatum. Scale bar = 500 μm. (C) Relationship between the instantaneous spike frequency (as the inverse of inter-spike interval) and time for different current amplitudes for the cell shown in A1. (D) Current–voltage relationship of the cell shown in A. Deviations of the potential from the extrapolated ohmic responses close to resting potential reflect inward and outward rectification, respectively.

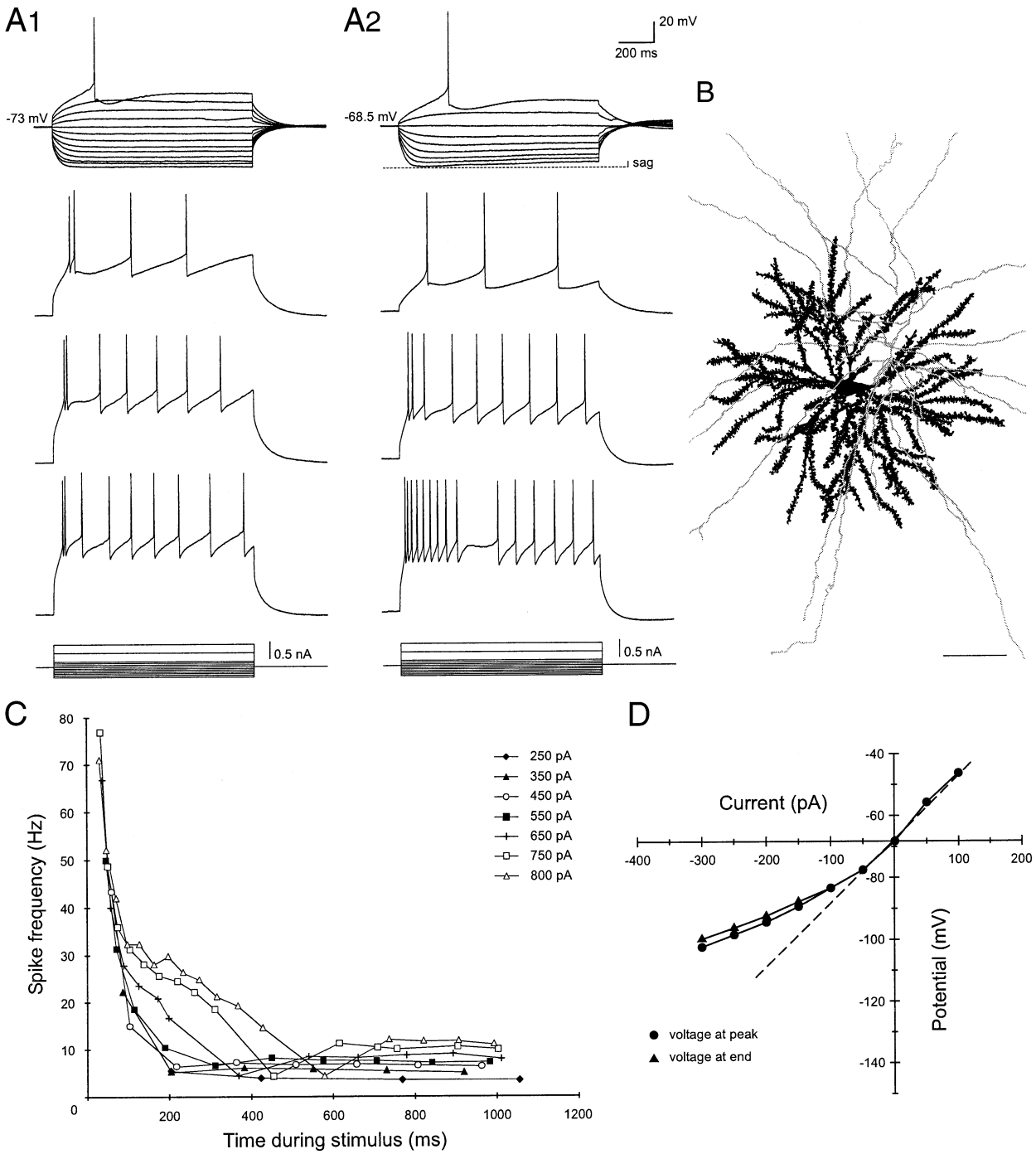

Fig. 3. Intrinsic firing properties and membrane rectification of type II neurons. (A) Examples of voltage responses to hyperpolarizing and depolarizing current pulses (−300–700 pA) in two neurons that showed a phasic-tonic firing of action potentials over long depolarizing current. The cell in A1 displays fast inward rectification to hyperpolarizing current pulses. The cell in A2 shows the same fast inward rectification and additionally a sag in the voltage response to relatively large hyperpolarizing current pulses, resulting in a rebound overshoot at cessation of current pulses. See text for details. (B) Camera lucida reconstruction of a type II neuron. The soma and dendrites are drawn in black, the local axon collaterals are shown in gray. Scale bar = 50 μm. (C) Relationship between the instantaneous spike frequency and time for different current amplitudes for the cell shown in A2. After a phasic response the spike frequency rapidly adapts to a steady-state tonic firing. (D) Current–voltage relationship of the cell shown in A2. ●, voltage response measured at the end of the current pulse; ▲, voltage at the peak.

phasic-tonic firing emerged in which a train of action potentials followed a short burst. This train of action potentials showed conspicuous frequency adaptation (Fig. 3A, lower traces, and Fig. 3C), but the repetitive firing pattern could be sustained at low frequencies (between 5 and 15 Hz) over long depolarizing current pulses (see also Fig. 4 for differences between type I and II neurons). A comparatively negative action potential threshold (Table 1) facilitated this firing behavior. A number of type II cells (29 of 49) showed the same sequence of afterpotentials following an action potential as described for the subset of type I neurons above.

Membrane rectification. Among the four types identified, type II neurons had the lowest input resistance and an intermediate membrane time constant (Table 1). Type II cells differed with regard to the existence of a hyperpolarization-activated time-dependent inward rectification: when hyperpolarizing current pulses were applied to type II cells a fast-activated inward rectifying conductance appeared at membrane potentials more negative than about −80 mV (Fig. 3A1). This inward rectification resulted in a slight upward bend in the hyperpolarized portion of the current–voltage plot when compared with the extrapolated linear portion (Fig. 3D, voltage at peak). In the majority of type II neurons (37 of 49) in addition a small sag in the voltage response (3.1–8.1% sag) could be seen at potentials more negative than −80 mV. This delayed inward rectifying conductance pushed the membrane potential back towards resting values and led to a rebound overshoot at the termination of hyperpolarizing current pulses (Fig. 3A2). The amplitude of the sag increased with more hyperpolarized membrane potentials (Fig. 3D, voltage at end). These cells in addition seemed to possess the same fast-activated inward rectification seen in the remaining type II neurons (above) as their peak voltage responses exhibited inward rectification over the same range of membrane potentials as the time-dependent inward rectification (Fig. 3D). At depolarizing voltage steps the membrane potential often depolarized more than expected from the ohmic response around resting potential, indicating the contribution of an inward rectification in the voltage range close to spike threshold. During long current pulses the membrane potential sagged back towards rest (4.8–19.4% sag) resulting in a rebound undershoot at the termination of the current pulse (Fig. 3A2).

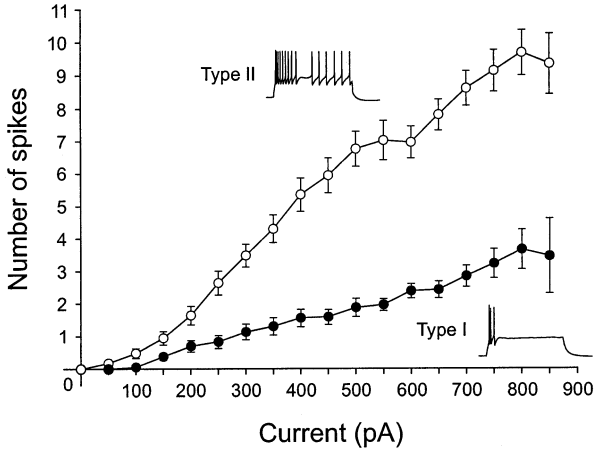

Fig. 4. Differences in firing patterns between type I neurons and type II neurons correlate with the sensitivity to current injection. Relationship between somatically injected depolarizing current and the number of evoked action potentials in type I ($n = 56$) and type II ($n = 49$) neurons. Type II neurons (open symbols) require a smaller amount of current to initiate action potential firing (rheobase) and are able to sustain firing during long depolarizing current pulses (cf. Table 1). Type I neurons on the other hand show complete firing arrest during prolonged depolarization. Data are means ± S.E.M.

Morphology. The morphology of 24 type II cells that were successfully recovered closely resembled that of type I cells (Figs. 3B, 6C, D and 7). They had large oblique somata (diameter 16–23 μm; Table 2) and long, thick multipolar dendrites. The dendrites of type II neurons had a similar number of branch points and displayed an equally high number of spines as type I neurons (Table 2). On average, the dendrites of type II cells were slightly longer than those of any cell type and they covered large areas (diameter of dendritic field 232–302 μm; Table 2). The axons of type II neurons often formed a radial axonal plexus in the vicinity of the soma giving rise to several local ramifications as well as long collaterals that projected to targets beyond the borders of the NCL. As in type I cells most neurons

Table 1. Electrophysiological characteristics of classes of neurons in the NCL (means ± S.E.M.)

	Type I ($n = 56$)	Type II ($n = 49$)	Type III ($n = 16$)	Type IV ($n = 15$)	Significant differences[a]
Resting potential (mV)	−76.7 (±0.6)	−73.7 (±0.7)	−64.0 (±1.2)	−67.5 (±1.1)	Type I > II > III, IV
Input resistance (MΩ)	186.1 (±11.5)	166.4 (±8.3)	470.5 (±24.5)	569.1 (±20.1)	Type IV > III > I, II
Membrane time constant (ms)	45.7 (±2.1)	39.1 (±2.1)	31.2 (±3.6)	93.0 (±7.7)	Type IV > I, II, III
Spike threshold (mV)	−30.9 (±0.5)	−33.8 (±0.5)	−37.8 (±0.8)	−27.1 (±0.7)	Type III > II > I > IV
Max. number of spikes (1.1 s depolarizing pulse)	3.8 (±0.4)	9.8 (±0.6)	43.6 (±4.1)	6.4 (±0.9)	Type III > II > I; type III > IV
Rheobase current (pA)	306.9 (±20.3)	225.0 (±13.1)	52.3 (±7.9)	76.7 (±9.4)	Type I > II > III, IV
Spike duration at half-amplitude (ms)	1.82 (±0.05)	1.70 (±0.06)	0.91 (±0.08)	2.23 (±0.1)	Type IV > I, II > III
Rise time (10–90%; ms)	0.67 (±0.02)	0.59 (±0.02)	0.44 (±0.04)	1.11 (±0.1)	Type IV > I, II; type I > III
Fall time (90–10%; ms)	1.49 (±0.04)	1.42 (±0.04)	0.93 (±0.07)	1.70 (±0.09)	Type IV > II > III; type I > III
Spike amplitude (mV)	58.2 (±1.4)	57.2 (±1.3)	49.4 (±2.8)	48.8 (±1.8)	Type I, II > III; type I > IV
AHP amplitude (mV)	−17.6 (±0.5)	−18.0 (±0.5)	−18.0 (±1.0)	−16.7 (±1.1)	–

[a]Significant differences indicated by the use of a Scheffe test for multiple comparisons after ANOVA ($P < 0.05$).

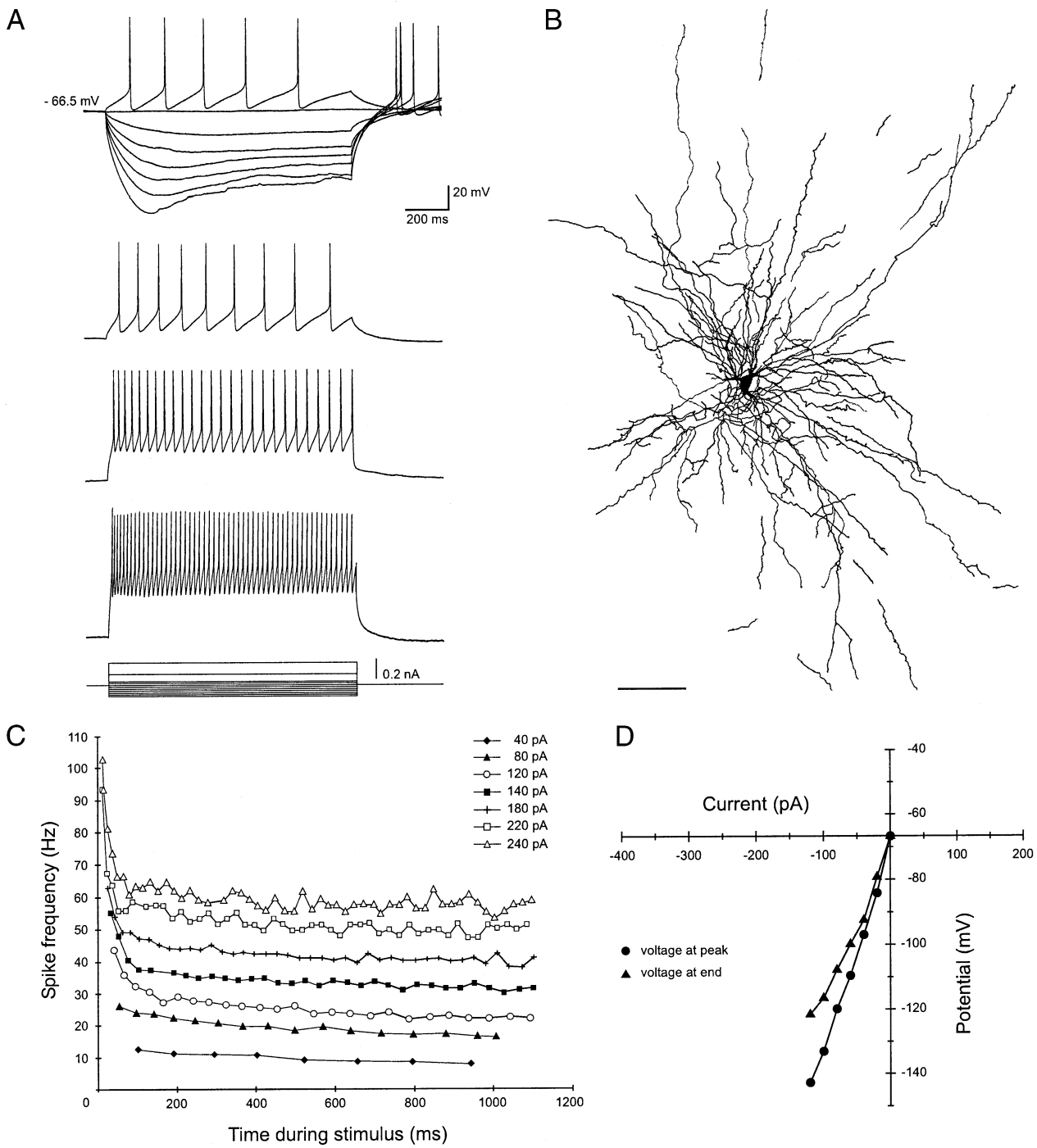

Fig. 5. Intrinsic firing properties and membrane rectification of a type III cell. (A) Voltage responses to hyperpolarizing and depolarizing current pulses (−120–240 pA). There is a large sag in response to strong hyperpolarizing current pulses, which results in a rebound overshoot that is large enough to trigger spikes. Small depolarizing currents elicit continuous firing at comparatively high frequencies. (B) Camera lucida reconstruction of a type III neuron. Scale bar = 50 μm. (C) Relationship between the instantaneous spike frequency and time for different current amplitudes for the cell shown in A. There is some frequency adaptation after the first few spikes, but the cell maintains a high-frequency firing without further attenuation over a long current pulse. (D) Current–voltage relationship of the cell shown in A. ●, voltage response measured at the end of the current pulse; ▲, voltage at the peak.

sent one to three descending collaterals towards the archistriatum but also had additional arborizations that seemed to travel ventromedially and dorsomedially (cf. Fig. 7, insert), probably making numerous contacts with other cells within NCL on their way.

Type III neurons

The key features of type III neurons were the ability to fire action potentials at a high frequency and a prominent sag in the response to hyperpolarizing current

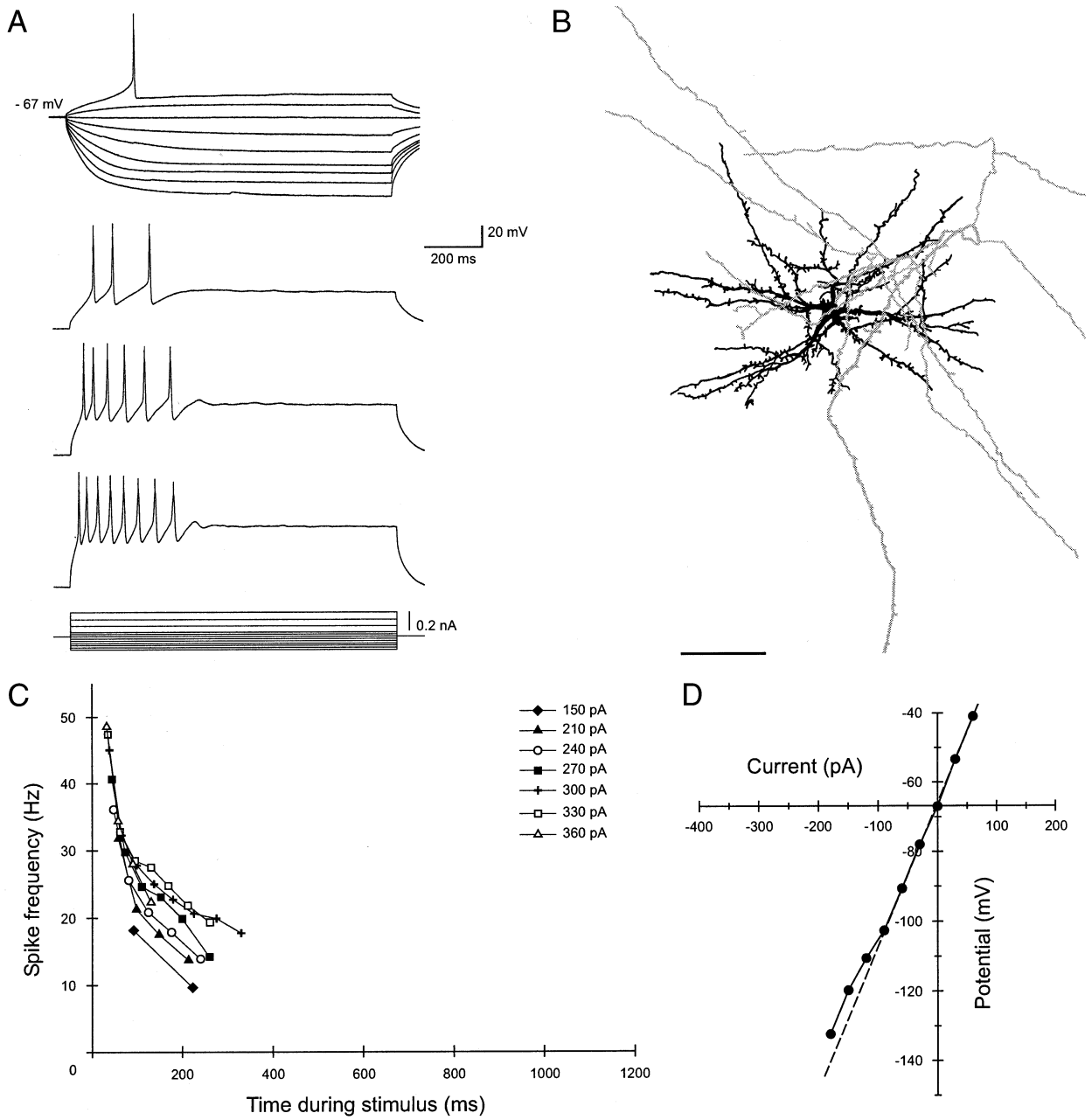

Fig. 6. Intrinsic firing properties and membrane rectification of a type IV cell. (A) Voltage responses to hyperpolarizing and depolarizing current pulses (−180–360 pA). The cell shows large voltage responses to small hyperpolarizing current pulses with relatively little inward rectification. Small depolarizing current pulses readily elicit short bursts of action potentials. (B) Camera lucida reconstruction of a type IV neuron. The soma and dendrites are drawn in black, the axon collaterals are shown in gray. Scale bar = 50 μm. (C) Relationship between the instantaneous spike frequency and time for different current amplitudes for the cell shown in A. (D) Current–voltage relationship of the cell shown in A. The input resistance is high, and the voltage response shows only little inward rectification to large current pulses.

pulses, as well as a short action potential duration. Type III cells represented 16 of the 136 cells (12%) characterized.

Firing properties. In response to small suprathreshold depolarizing current pulses all neurons designated as type III responded with regular tonic firing that showed only relatively little frequency adaptation (Fig. 5). Thus, type III cells were able to initially fire action potentials at frequencies of about 100 Hz. After several spikes the firing rate usually accommodated to some degree, but sustained firing over long depolarizing current pulses continued at frequencies much higher than found in any other cell class (Fig. 5C). These cells also showed the most positive RMPs, while generally having the most negative threshold for the initiation of an action potential (Table 1). The duration of action potentials in type III cells was by far the shortest among all classes, which was also reflected by short rise and fall times (Table 1). The action potential was followed by an

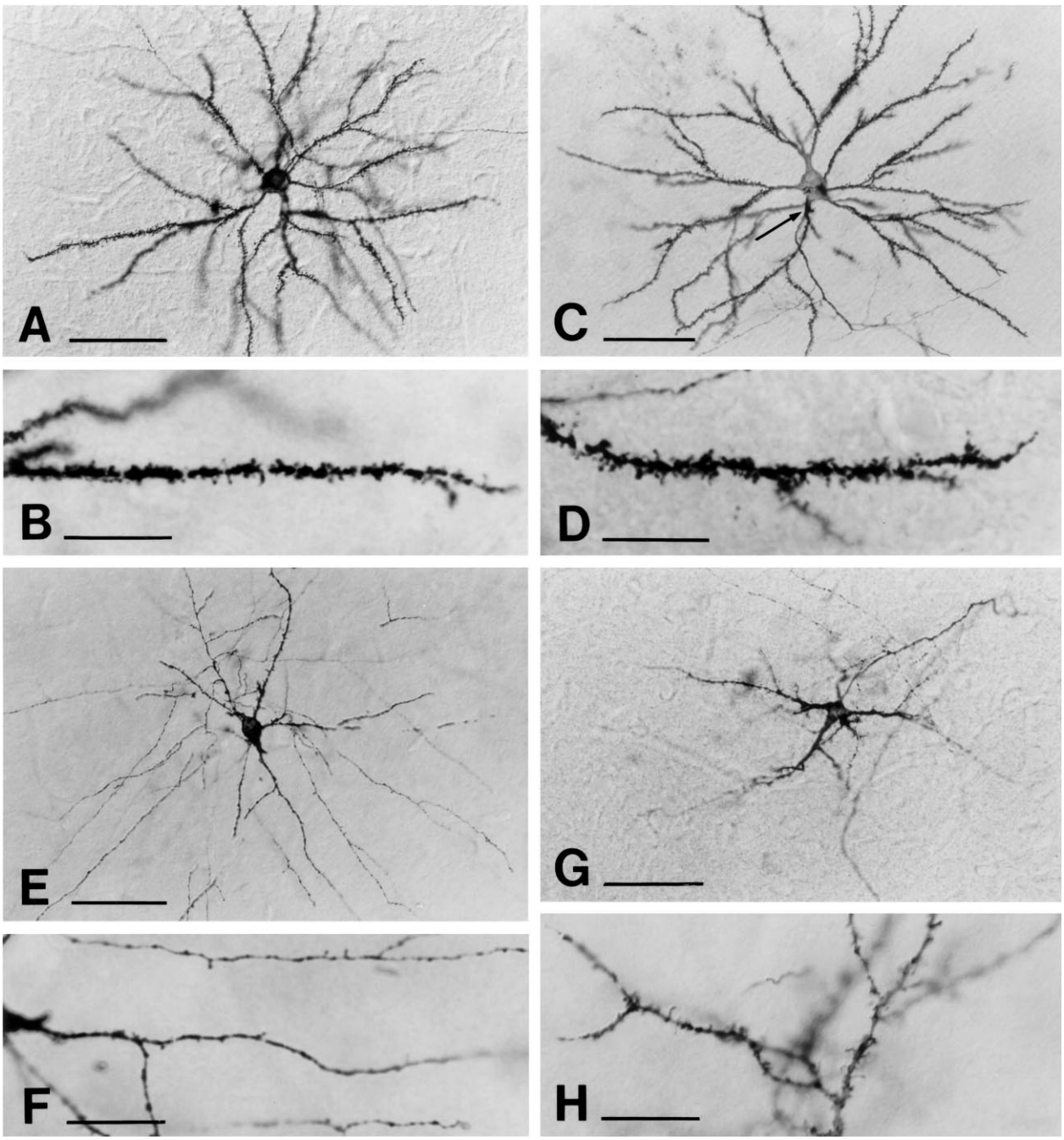

Fig. 7. Morphological features of cell types in the NCL of the chick. (A–H) Photomicrographs of LY-filled neurons that were classified according to their electrophysiological properties following somatic current injection (see text for details). (A) Example of a neuron that responded to depolarizing current pulses with rapidly adapting bursts of action potentials (type I). (B) Detail of a dendrite with numerous spines from another type I cell. (C) Example of a neuron that responded with phasic-tonic firing of action potentials in response to depolarizing currents (type II). The arrow points to where the axon leaves the cell body. (D) Detail of a type II cell showing a dendrite with numerous spines and part of an axon (top left). (E) Example of a sparsely spineous type III cell. (F) Detail of the cell shown in E. In the center of the photomicrograph is a dendrite; parallel to this run axon collaterals above and below. (G) Example of a cell that had high input resistance, small action potentials of long duration and showed only little inward rectification to hyperpolarizing current pulses (type IV). (H) Detail of the dendrites of another type IV cell. Scale bars = 50 μm (A, C, E, G), and 20 μm (B, D, F, H).

AHP that was large in amplitude compared to the relatively small amplitude of the spike (Table 1).

Membrane rectification. Type III cells had comparatively high input resistances but short membrane time constants (Table 1). In response to hyperpolarizing current pulses (membrane potential more negative than −80 mV) a prominent sag in the voltage response (9–21.5% sag) occurred that was followed by a rebound depolarization at cessation of the current pulse. The time-dependent inward rectification and the rebound overshoot increased as the hyperpolarizing current pulses increased.

In response to larger negative current pulses the rebound depolarization could initiate action potentials (Fig. 5A). Type III neurons also appear to possess an additional fast-activated inward rectifier, as the peak voltage responses exhibited inward rectification over the same range of membrane potentials as the time-dependent inward rectification (Fig. 5D).

Morphology. Type III cells ($n = 7$) were characterized by small fusiform somata (diameter 10–14 μm; Table 2) and thin, aspiny or sparsely spiny dendrites (Figs. 5B, 7E, F and 8). In fact, in three out of seven neurons that were successfully reconstructed the dendrites were so thin that they could not be clearly distinguished from the extensive local axonal ramifications. The remaining three cells had relatively few long multipolar dendrites (diameter of dendritic field 227–267 μm). The dendrites showed a low number of total branch points and especially few higher order (≥ fourth branches) branchings (Table 2). The axon appeared to have a large number of varicosities, and arborized extensively to form a dense plexus of terminals in the vicinity of the soma (Figs. 7E and 8). Several long protruding axon collaterals formed symmetrical round or oval axonal fields with diameters of about 545–736 μm. Axons of type III neurons could never be followed beyond the borders of the NCL.

Type IV neurons

The key features of type IV cells are a high input resistance and long membrane time constant, as well as long action potential duration. Of the 136 cells characterized, 15 (11%) were found to belong to this class.

Firing properties. Among the classes identified here type IV cells had an intermediate RMP and a high spike threshold. Their bursting spike pattern resembled that of type I cells (Fig. 6), but type IV neurons were able to initially fire a larger number of action potentials (Table 1). However, in response to large depolarizing currents the ability of type IV neurons to fire repetitively was markedly attenuated (Fig. 6C). A characteristic of cells in this class was the long action potential duration, which was also reflected in the significantly longest rise and fall times (Table 1). Furthermore, the action potentials of type IV cells showed a prominent progressive spike broadening during repetitive firing. Type IV cells had comparatively small monophasic AHPs (Table 1).

Membrane rectification. The key feature required for type IV cells was a long membrane time constant (> 65 ms). They also had the highest input resistance (> 400 MΩ) among all classes of cells (Table 1) and showed steep current–voltage relationships (Fig. 6C). Only at membrane potentials more negative than −95 mV in most neurons a weak, fast-activated inward rectification became evident (Fig. 6D). All type IV cells showed a prominent membrane outward rectification at depolarized potentials but no sag.

Morphology. Type IV cells ($n = 9$) were characterized by small, oblique somata (diameter 12–16.5 μm; Table 2) and multipolar dendrites that possessed few thin spines. Usually, proximal dendrites were short and thin, but sometimes two or three main dendrites were seen that had thick stems but tapered considerably with distance from the soma (Figs. 6B and 7G). In these instances the usual spherical form of the dendritic field (diameter 180–225 μm) was tilted by these dendrites. The dendritic tree of type IV neurons showed relatively few branches and covered the smallest area among the four cell types (Table 2). Axonal arborizations of type IV cells were not as extensive as in type I or type II cells, but projections followed the same pattern seen in the other classes of spiny neurons. One to three main collaterals

Table 2. Morphological characteristics of classes of neurons in the NCL (means ± S.E.M.)

	Type I ($n = 30/n = 14$)[b]	Type II ($n = 24/n = 14$)[b]	Type III ($n = 7/n = 3$)[b]	Type IV ($n = 9/n = 9$)[b]	Significant differences[a]
Soma size (μm^2)	210.0 (± 9)	225.9 (± 9)	111.6 (± 6)	137.0 (± 12)	Type I, II > type III, IV
Total dendritic length (μm)	5438 (± 266)	6123 (± 278)	2624 (± 48)	2769 (± 404)	Type I, II > type III, IV
Area of dendritic arborizations (μm^2)	52386 (± 2469)	60436 (± 3172)	45975 (± 1608)	29250 (± 2709)	Type I, II > type IV
Number of dendrites	6.05 (± 0.34)	6.31 (± 0.34)	4.0 (± 0.57)	4.33 (± 0.33)	Type II > IV
Number of branch points	54.3 (± 1.7)	55.0 (± 2.5)	26.2 (± 1.8)	31.1 (± 2.2)	Type I, II > type III, IV
Number of spines (n/10 μm) initial segment	1.46 (± 0.29)	1.86 (± 0.39)	0.1 (± 0.1)	1.57 (± 0.43)	–
Second branching	5.61 (± 0.54)	6.08 (± 0.43)	1.30 (± 0.38)	2.69 (± 0.49)	Type I, II > type III, IV
Third branching	7.35 (± 0.53)	7.55 (± 0.47)	1.74 (± 0.36)	2.69 (± 0.60)	Type I, II > type III, IV
Fourth branching	8.24 (± 0.68)	8.02 (± 0.57)	0.56 (± 0.01)	2.75 (± 0.56)	Type I, II > type III, IV
Fifth and sixth branching	9.71 (± 0.78)	9.07 (± 1.03)	–	2.92 (± 0.82)	n.a.
Direction of axon	ventrally, dorsomedially, and ventromedially	ventrally, dorsomedially, and ventromedially	locally	ventrally, dorsomedially, and ventromedially	

[a]Significant differences indicated by the use of a Scheffe test for multiple comparisons after ANOVA ($P < 0.05$).
[b]The first number denotes the total number of cells that were analyzed for each cell type, the second number is the number of cells in which values for the distribution of spines across the dendritic tree were obtained. n.a.: not applicable since not enough cases for statistical comparison.

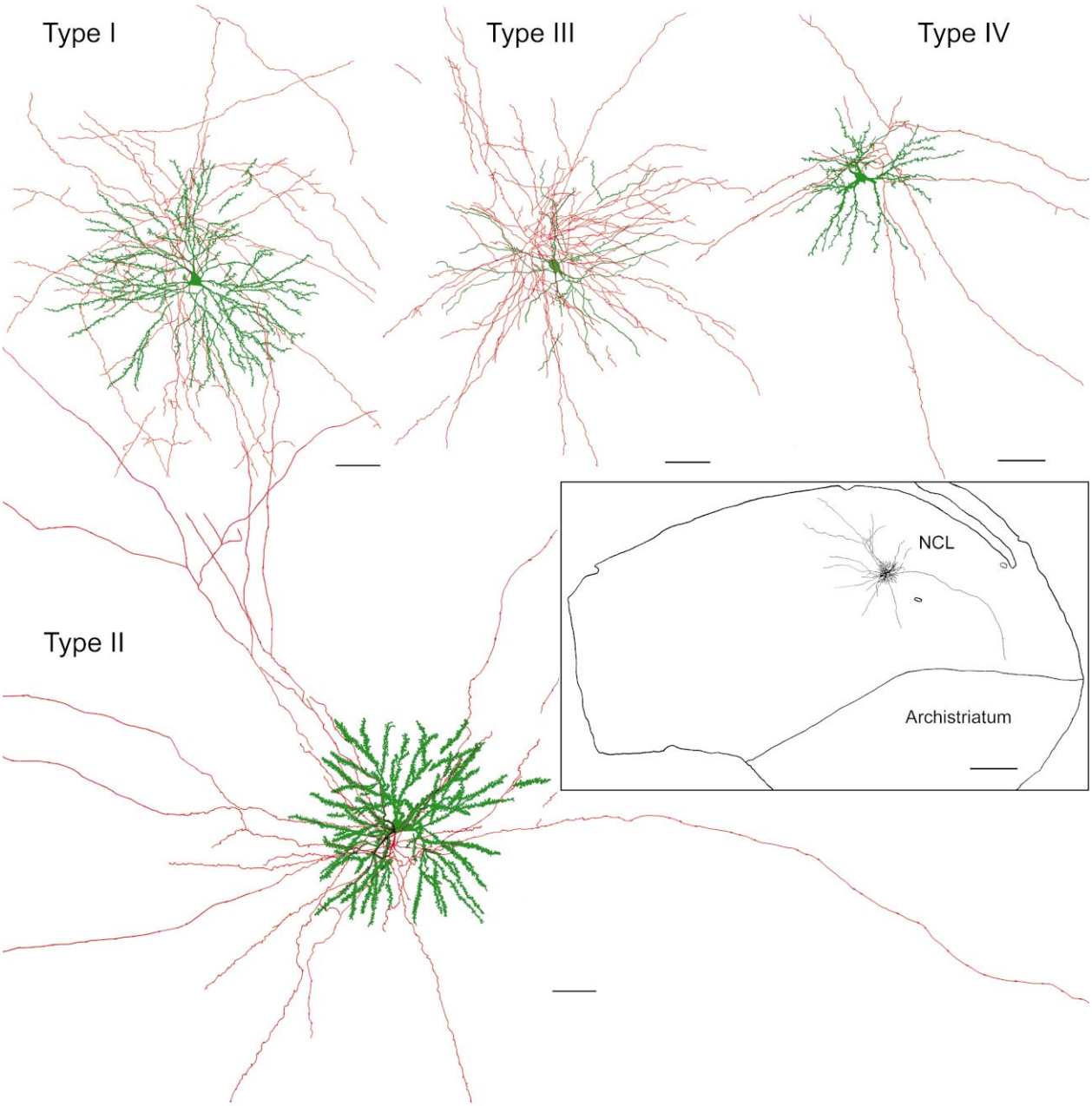

Fig. 8. Comparison of the dendritic morphology and the local axonal arborizations in the four cell types of NCL. Somata and dendrites are drawn in green, axon collaterals in red. With regard to spine density and dendritic thickness the examples shown here for the type I and type II neurons represent extremes of what appeared to be a continuum. Scale bars = 50 μm. Insert: low power reconstruction of the same type II neuron showing its position in the NCL. In addition to recurrent local arborizations most neurons from all spiny cell classes possessed one or several axon collaterals that left the NCL ventrally towards the archistriatum, ventromedially, in the direction of the basal ganglia, and/or dorsomedially, possibly to provide feedback to sensory and associative forebrain areas. Scale bar = 500 μm.

descended ventrally in the direction of the archistriatum, while other collaterals traveled dorsomedially and/or ventromedially within the NCL.

DISCUSSION

We have shown the existence of at least four cell types within the NCL of chicks based on their intrinsic electrophysiological and morphological properties. In general, there was a good correspondence of physiological and morphological criteria, although the two main types of projection neurons, types I and II, could not be differentiated by morphological criteria.

Cell types

Type I. Type I neurons possess a depolarized action potential threshold despite a relatively negative resting potential, and a prominent outward rectification in

response to depolarizing current pulses. These properties indicate that strong, temporally or spatially integrated excitatory inputs are necessary for type I neurons to fire. If sufficiently depolarized, cells in this class preferentially responded with bursts of action potentials. Functionally, a neuron's ability to fire bursts of action potentials will probably enhance its integrative role within a network and aide the plasticity of synaptic connections: burst firing may increase the probability of driving the post-synaptic cell beyond spike threshold (Snider et al., 1998). The high-frequency firing of action potentials during a burst is thus thought to amplify a neural signal and to synchronize the activity in a population of post-synaptic cells, both temporarily and spatially (Snider et al., 1998; Williams and Stuart, 1999). In a set of type I and type II neurons single action potentials or bursts were followed by three distinct afterpotentials, consisting of an initial fast, and a late slow afterhyperpolarization, separated by an intercalated depolarizing afterpotential. Depolarizing afterpotentials appear to be related to a neuron's ability to fire bursts of action potentials (Chagnac-Amitai et al., 1990; Magee and Carruth, 1999). In mammals, the expression of the afterpotential and the emergence of a tripartite AHP have been shown to depend on changes during post-natal development, and similarly, burst firing does not develop before the third post-natal week (Kasper et al., 1994). In contrast, chicks are already well developed at hatch; accordingly, we observed evoked bursts in recordings from very young animals (2 days post-hatch, data not shown).

Type II. An initial tonic firing and a relatively hyperpolarized action potential threshold may indicate that the firing of type II cells is readily elicited by weak excitatory inputs. The phasic-tonic firing pattern elicited with large depolarizing currents indicates that type II neurons respond strongly but transiently to a brief input, yet produce a sustained response to a prolonged input; a pattern that favors the augmentation of synaptic connections (Thomson, 2000). Functionally, the ability to generate a tonic firing mode could also enable type II cells to retain information of their input for a short time period. Pharmacological blockade or lesions of the NCL in pigeons cause specific impairments in a variety of delay tasks (Mogensen and Divac, 1982, 1993; Gagliardo et al., 1996, 1997; Güntürkün, 1997; Diekamp et al., 2000; Güntürkün and Durstewitz, 2000). In these experiments, the animal has to hold on-line specific information provided during a previous cue period to perform a correct response after the end of the delay. In mammals, neurons in the prefrontal cortex show enhancement in their firing rate during the delay (e.g. Funahashi et al., 1989). The sustained delay activity of these neurons may provide the animal with the ability to hold an internal representation of relevant aspects of the external world that are needed for the organization of subsequent responses (Goldman-Rakic, 1996). Neurons with similar delay activities to those recorded from rat or primate prefrontal cortex have been observed in the pigeon's NCL during a delayed Go/No-Go task (Kalt et al., 1999). The ability of type II neurons to sustain firing over long periods of time makes them likely candidates to participate in the maintenance of sustained delay activity within the NCL.

The majority of type II neurons furthermore showed a small transient sag in the voltage response to hyperpolarizing currents, which was never seen in type I or IV neurons. This inward rectification is likely to be mediated by a voltage- and time-dependent hyperpolarization-activated mixed cationic current called I_h (Pape, 1996; see also discussion of type III below). It has been shown that neurons with a time-dependent-inward rectifier fire action potentials preferentially to rhythmic (oscillatory) inputs (Hutcheon et al., 1996). Recently, neurons have been described in the dorsal forebrain of zebra finches, which participate in the perception of song pattern, and which share a number of firing properties and morphological features with the type II neurons in the present study (Dutar et al., 1998; Kubota and Taniguchi, 1998; Mooney, 2000). Thus, type II neurons may represent members of a common class of spiny projection neurons in the dorsal forebrain of birds that can respond preferentially to input of a specific pattern.

Type III. The electrophysiological and morphological characteristics of the type III cells resemble those of GABA-containing inhibitory interneurons found in the mammalian telencephalon (McCormick et al., 1985; Kawaguchi, 1995; Gupta et al., 2000), i.e. little or no accommodation of spike frequency, and beaded aspiny dendrites. Type III cells are capable of sustained firing of action potentials at a wide range of frequencies. They are thus able to perform a very reliable input–output conversion, retaining the temporal pattern of their synaptic inputs. These firing characteristics are facilitated by the short rise and fall times of the action potential (Table 1). In addition, the relatively pronounced AHPs of type III cells may also enable sustained high-frequency firing of action potentials in that they reduce the accumulation of depolarization-dependent Na^+ channel inactivation (Hamill et al., 1991; Erisir et al., 1999). Large AHPs will also reduce the influx of Ca^{2+} into the cell, thus diminishing the effects of Ca^{2+}-activated K^+ channels, which otherwise might lead to prolonged hyperpolarization and spike frequency adaptation (Storm, 1990). Another prominent feature in type III cells is the existence of the strong inward rectifying current I_h that initiates slow depolarization if the membrane potential has become negative. In central neurons of mammals I_h has been implicated in the determination of the resting potential and the generation of 'pacemaker' potentials. It also serves to decrease the propagation of subthreshold voltage potentials in dendritic trees, thereby regulating the integration of synaptic inputs (Magee, 1998, 1999). In mammalian cortex GABAergic interneurons have long been recognized for controlling the spread of activity (Chagnac-Amitai and Connors, 1989), and the synchronization of adjacent projection neurons via inhibitory phasing (Cobb et al., 1995; Benardo, 1997), which might impose a rhythm on the activity of the principal neurons (Buzsáki and Chrobak, 1995). With respect to

the extensive local axonal arborizations of type III neurons these putative interneurons of the NCL appear to be able to control a large number of adjacent spiny 'principal' neurons. In summary, given their intrinsic electrophysiological and morphological properties type III neurons of the NCL are equipped to play a similarly important role for signal integration as their mammalian counterparts.

Type IV. Type IV neurons are characterized by high input resistances, long time constants and a long duration of action potentials. A high input resistance and long membrane time constant could increase the magnitude and duration of a cell's response to imposed synaptic currents. These electrophysiological properties most likely result from the morphology of type IV neurons, which possesses small somata, and short, sparsely spineous dendrites with few branchings. This morphology should render type IV neurons electrotonically compact, and reduce cable attenuation of distal dendritic synaptic inputs. This could compensate for the comparatively small number of synaptic inputs that these neurons receive. Similarly, the long duration of action potentials seen in type IV neurons may serve to facilitate their output: activity-dependent spike broadening due to a reduction in specific K^+ currents has been correlated with increased efficacy of synaptic transmission onto the post-synaptic target cell (see Byrne and Kandel, 1996 for review). Similarly, the significantly longer action potentials of developing neurons might result in an enhancement of synaptic transmission onto their post-synaptic cells. It should also be noted that a high input resistance, long time constant and a long duration of action potentials are also characteristics of developing cortical neurons in mammals (McCormick and Prince, 1987; Kasper et al., 1994) and possibly birds (Kubota and Taniguchi, 1998). It is thus also conceivable that type IV neurons represent a class of late maturing neurons.

Connectivity and sensorimotor integration

The pattern of axonal arborizations described for the four cell types here may provide further insight into the anatomical arrangements that underlie (a) the integration of various sensory modalities within the NCL, and (b) the control of motor and limbic areas via the NCL's descending projections, as they have been indicated from the results of tracing studies *in vivo* (Metzger et al., 1998; Kröner and Güntürkün, 1999). Overlap in the termination areas of sensory afferents indicates that in large areas of the NCL single neurons might receive multimodal input. In agreement with this, single-unit recordings *in vivo* show that neurons in the NCL of the pigeon can encode aspects of a memory task across modalities (Kalt et al., 1999). The present data indicate that individual cells, or a few interconnected neurons, can provide for stimulus comparison across most sensory compartments of the NCL (cf. Metzger et al., 1998; Kröner and Güntürkün, 1999), either through their extensive local axonal arborizations or the long collaterals that span the whole mediolateral and/or dorsoventral extent of the NCL. It must be noted, however, that the determination of the rostrocaudal extent of these intra-NCL connections remains a critical topic, which was constrained by the thickness of the slices used here.

The long axon collaterals of NCL neurons of all types showed similar projection patterns, thus suggesting that they innervate common targets. The trajectories of these efferents followed general patterns outlined in previous tracing studies *in vivo* (Metzger et al., 1998; Kröner and Güntürkün, 1999). Individual projection neurons of the NCL thus appear to provide feedback to sensory areas and/or send parallel efferent copies to the limbic and motor regions in the archistriatum and the basal ganglia, respectively. The latter finding is also noteworthy with regard to comparisons with the organization of the caudal forebrain in other birds. Based on similarities in the pattern of connections and the location in the dorsocaudal forebrain it has previously been suggested that the Nd, the auditory subunit of the NCL, may be related to the HVC (used as the proper name) of songbirds (Wild, 1994; Metzger et al., 1998; Kröner and Güntürkün, 1999). The HVC is involved in the production of song and gives rise to two pathways that terminate in a motor nucleus of the archistriatum and the so called area X of the basal ganglia (Nottebohm et al., 1982; Fortune and Margoliash, 1995). In the HVC of zebra finches these projections arise from two separate populations of neurons which resemble type I and type II neurons of the present study, respectively (Dutar et al., 1998; Kubota and Taniguchi, 1998). However, as pointed out above, our anatomical findings make it unlikely that a similar distinction between cell types exists in the chick forebrain. These differences might reflect the specialization of the HVC relevant for singing and the need to exert control over specific aspects of singing-related motor behavior. In summary, our findings provide a framework for further study into sensorimotor integration and associative learning in chicks and possibly other birds.

Acknowledgements—This work was supported by Grants of the DFG (GU 227/5-1 to O.G., and SFB 509 to K.G. and H.H.).

REFERENCES

Aldavert-Vera, L., Costa-Miserachs, D., Divac, I., Delius, J.D., 1999. Presumed 'prefrontal cortex' lesions in pigeons: effects on visual discrimination performance. Behav. Brain Res. 102, 165–170.

Benardo, L.S., 1997. Recruitment of GABAergic inhibition and synchronization of inhibitory interneurons in rat neocortex. J. Neurophysiol. 77, 3134–3144.

Bock, J., Braun, K., 1999a. Blockade of *N*-methyl-D-aspartate receptor activation suppresses learning-induced synaptic elimination. Proc. Natl. Acad. Sci. USA 96, 2485–2490.

Bock, J., Braun, K., 1999b. Filial imprinting in domestic chicks is associated with spine pruning in the associative area, dorsocaudal neostriatum. Eur. J. Neurosci. 11, 2566–2570.
Bock, J., Schnabel, R., Braun, K., 1997. Role of the dorso-caudal neostriatum in filial imprinting of the domestic chick: a pharmacological and autoradiographical approach focused on the involvement of NMDA-receptors. Eur. J. Neurosci. 9, 1262–1272.
Braun, K., Bock, J., Metzger, M., Jiang, S., Schnabel, R., 1999. The dorsocaudal neostriatum of the domestic chick: a structure serving higher associative functions. Behav. Brain Res. 98, 211–218.
Buzsáki, G., Chrobak, J.J., 1995. Temporal structure in spatially organized neuronal ensembles: a role for interneuronal networks. Curr. Opin. Neurobiol. 5, 504–510.
Byrne, J.H., Kandel, E.R., 1996. Presynaptic facilitation revisited: state and time dependence. J. Neurosci. 16, 425–435.
Chagnac-Amitai, Y., Connors, B.W., 1989. Horizontal spread of synchronized activity in neocortex and its control by GABA mediated inhibition. J. Neurophysiol. 61, 747–758.
Chagnac-Amitai, Y., Luhmann, H.J., Prince, D.A., 1990. Burst generating and regular spiking layer 5 pyramidal neurons of rat neocortex have different morphological features. J. Comp. Neurol. 296, 598–613.
Cobb, S.R., Buhl, E.H., Halasy, K., Paulsen, O., Somogyi, P., 1995. Synchronization of neuronal activity in hippocampus by individual GABAergic interneurons. Nature 378, 75–78.
Diekamp, B., Kalt, T., Ruhm, A., Koch, M., Güntürkün, O., 2000. Impairment in a discrimination reversal task after D1 receptor blockade in the pigeon 'prefrontal cortex'. Behav. Neurosci. 114, 1145–1155.
Douglas, R.J., Martin, K.A.C., 1992. In search of the canonical microcircuits of neocortex. In: Lent, R. (Ed.), The Visual System from Genesis to Maturity. Birkhäuser, Boston, MA, pp. 213–232.
Dutar, P., Vu, H.M., Perkel, D.J., 1998. Multiple cell types distinguished by physiological, pharmacological, and anatomic properties in nucleus HVc of the adult zebra finch. J. Neurophysiol. 80, 1828–1838.
Erisir, A., Lau, D., Rudy, B., Leonard, C.S., 1999. Function of specific K^+ channels in sustained high-frequency firing of fast-spiking neocortical interneurons. J. Neurophysiol. 82, 2476–2489.
Fortune, E.S., Margoliash, D., 1995. Parallel pathways and convergence onto HVc and adjacent neostriatum of adult zebra finches (*Taeniopygia guttata*). J. Comp. Neurol. 360, 413–441.
Foster, T.M., Temple, W., MacKenzie, C., Demello, L.R., Poling, A., 1995. Delayed matching-to-sample performance of hens. Effects of sample duration and response requirements during the sample. J. Exp. Anal. Behav. 64, 19–31.
Funahashi, S., Bruce, C.J., Goldman-Rakic, P.S., 1989. Mnemonic coding of visual space in the monkey's dorsolateral prefrontal cortex. J. Neurophysiol. 61, 331–349.
Gagliardo, A., Divac, I., 1993. Effects of ablation of the presumed equivalent of the mammalian prefrontal cortex on pigeon homing. Behav. Neurosci. 107, 280–288.
Gagliardo, A., Bonadonna, F., Divac, I., 1996. Behavioural effects of ablations of the presumed 'prefrontal cortex' or the corticoid in pigeons. Behav. Brain Res. 78, 155–162.
Gagliardo, A., Mazzotto, M., Divac, I., 1997. Memory of radial maze behavior in pigeons after ablations of the presumed equivalent of mammalian prefrontal cortex. Behav. Neurosci. 111, 955–962.
Goldman-Rakic, P.S., 1996. Regional and cellular fractionation of working memory. Proc. Natl. Acad. Sci. USA 93, 13473–13480.
Güntürkün, O., 1997. Cognitive impairments after lesions of the neostriatum caudolaterale and its thalamic afferent in pigeons: Functional equivalencies to the mammalian prefrontal system? J. Brain Res. 1, 133–144.
Güntürkün, O., Durstewitz, D., 2000. Multimodal areas in the avian forebrain – blueprints for cognition? In: Roth, G., Wullimann, M. (Eds.), Brain Evolution and Cognition. Spektrum Akademischer Verlag, pp. 431–450.
Gupta, A., Wang, Y., Markram, H., 2000. Organizing principles for a diversity of GABAergic interneurons and synapses in the neocortex. Science 287, 273–278.
Hamill, O.P., Huguenard, J.R., Prince, D.A., 1991. Patch-clamp studies of voltage-gated currents in identified neurons of the rat cerebral cortex. Cereb. Cortex 1, 48–61.
Hartmann, B., Güntürkün, O., 1998. Selective deficits in reversal learning after neostriatum caudolaterale lesions in pigeons – possible behavioral equivalencies to the mammalian prefrontal system. Behav. Brain Res. 96, 125–133.
Hutcheon, B., Miura, R.M., Puil, E., 1996. Subthreshold membrane resonance in neocortical neurons. J. Neurophysiol. 76, 683–697.
Kalt, T., Diekamp, B., Güntürkün, O., 1999. Single unit activity during a Go/NoGo task in the 'prefrontal cortex' of pigeons. Brain. Res. 839, 263–278.
Kasper, E.M., Larkman, A.U., Lübke, J., Blakemore, C., 1994. Pyramidal neurons in layer 5 of the rat visual cortex. II. Development of electrophysiological properties. J. Comp. Neurol. 339, 475–494.
Kawaguchi, Y., 1995. Physiological subgroups of nonpyramidal cells with specific morphological characteristics in layer II/III of rat frontal cortex. J. Neurosci. 15, 2638–2655.
Kröner, S., Güntürkün, O., 1999. Afferent and efferent connections of the caudolateral neostriatum in the pigeon (*Columba livia*): A retro- and anterograde pathway tracing study. J. Comp. Neurol. 407, 228–260.
Kubota, M., Taniguchi, I., 1998. Characteristics of classes of neuron in the HVc of the zebra finch. J. Neurophysiol. 80, 914–923.
Leutgeb, S., Husband, S., Riters, L.V., Shimizu, T., Bingman, V.P., 1996. Telencephalic afferents to the caudolateral neostriatum of the pigeon. Brain Res. 730, 173–181.
Magee, J.C., 1998. Dendritic hyperpolarization-activated currents modify the integrative properties of hippocampal CA1 pyramidal neurons. J. Neurosci. 18, 7613–7762.
Magee, J.C., 1999. Dendritic I_h normalizes temporal summation in hippocampal CA1 neurons. Nat. Neurosci. 2, 508–514.
Magee, J.C., Carruth, M., 1999. Dendritic voltage-gated ion channels regulate the action potential firing mode of hippocampal CA1 pyramidal neurons. J. Neurophysiol. 82, 1895–1901.
McCormick, D.A., Prince, D.A., 1987. Post-natal development of electrophysiological properties of rat cerebral cortical pyramidal neurones. J. Physiol. 393, 743–762.
McCormick, D.A., Connors, B.W., Lighthall, J.W., Prince, D.A., 1985. Comparative electrophysiology of pyramidal and sparsely spiny stellate neurons of the neocortex. J. Neurophysiol. 54, 782–806.
Metzger, M., Jiang, S., Braun, K., 1998. Organization of the dorsocaudal neostriatal complex: a retrograde and anterograde tracing study in the domestic chick with special emphasis on pathways relevant to imprinting. J. Comp. Neurol. 395, 380–404.
Mogensen, J., Divac, I., 1982. The prefrontal 'cortex' in the pigeon: Behavioral evidence. Brain Behav. Evol. 21, 60–66.
Mogensen, J., Divac, I., 1993. Behavioural effects of ablation of the pigeon-equivalent of the mammalian prefrontal cortex. Behav. Brain Res. 55, 101–107.
Mooney, R., 2000. Different subthreshold mechanisms underlie song selectivity in identified HVc neurons of the zebra finch. J. Neurosci. 20, 5420–5436.

Nottebohm, F., Kelley, D.B., Paton, J.A., 1982. Connections of vocal control nuclei in the canary telencephalon. J. Comp. Neurol. 207, 344–357.
Pape, H.C., 1996. Queer current and pacemaker: the hyperpolarization-activated cation current in neurons. Annu. Rev. Physiol. 58, 299–327.
Snider, R.K., Kabara, J.F., Roig, B.R., Bonds, A.B., 1998. Burst firing and modulation of functional connectivity in cat striate cortex. J. Neurophysiol. 80, 730–744.
Storm, J.F., 1990. Potassium currents in hippocampal pyramidal cells. Prog. Brain Res. 83, 161–187.
Thomson, A.M., 2000. Facilitation, augmentation and potentiation at central synapses. Trends Neurosci. 23, 305–312.
Vallortigara, G., Regolin, L., Rigoni, M., Zanforlin, M., 1998. Delayed search for a concealed imprinted object in the domestic chick. Anim. Cog. 1, 17–24.
Wild, J.M., 1994. Visual and somatosensory inputs to the avian song system via nucleus uvaeformis (Uva) and a comparison with the projections of a similar thalamic nucleus in a nonsongbird (*Columba livia*). J. Comp. Neurol. 349, 512–535.
Williams, S.R., Stuart, G.J., 1999. Mechanisms and consequences of action potential burst firing in rat neocortical pyramidal neurons. J. Physiol. 521, 467–482.

(*Accepted* 27 *September* 2001)